Soft Matter

PAPER

View Article Online
View Journal | View Issue

Cite this: *Soft Matter*, 2022, **18**, 5960

Multi-layer 3D printed dipeptide-based low molecular weight gels†

Max J. S. Hill and Dave J. Adams *

Received 19th May 2022,
Accepted 22nd July 2022

DOI: 10.1039/d2sm00663d

rsc.li/soft-matter-journal

We describe the direct 3D printing of dipeptide hydrogels, forming layers from gels prepared from different dipeptides. The dipeptides self-assemble into fibres that lead to very different microstructures letting us differentiate between the gels. We show how the mechanical properties of the overall 3D printed structures are affected by the composition of each of the layers, allowing us to build up structures with different microstructure and stiffness. We also discuss the interface between layers formed from different gelators, showing that the gels remain independent from neighbouring printed material, even when prepared in very close proximity.

Introduction

3D printing allows for the sequential deposition of pre-designed layers of material to create desired structures.[1] Whilst heated plastic filaments are traditionally used, extrusion-based 3D printers can be modified to allow for the effective 3D printing of hydrogels.[2,3] The controlled formation of hydrogels into well-defined patterns has applications in biomedical fields such as drug delivery and tissue engineering.[4–9] The extrusion of numerous hydrogels based on polymers and peptides has been well reported.[10] Typically, these gels are expelled as solutions that undergo gelation post printing *via* various triggers, such as a temperature change,[11] UV photocuring,[12–14] exposure to cross linking agents,[15] and printing into solutions or pre-existing gels.[16,17]

In contrast, examples of 3D printed low molecular weight gels in the literature are less common.[18] Such gels rely on reversible non-covalent interactions to fix their underlying networks. This reversibility enables the linkages within the network to be broken and reform, allowing the networks to recover after stress is applied.[19] This shear recovery along with the thixotropic nature of these gels gives them great potential for use as 3D bioprinting media. Unlike chemical gels, some supramolecular gels can be pre-formed and extruded,[20–22] instead of gelation solely occurring post-printing.[3,23,24] This conceptually enables the properties of the final printed material to be predefined by the gel chosen to be extruded.[20] However, this assumption is dependent on the gel being printable after formation and the effect of extrusion on the materials properties.[20,25]

Most examples of 3D printed low molecular weight gels are systems printed with layers formed from a single gelator.[18,20,23–25] Whilst a logical starting point with which to optimise material requirements and printing parameters,[20] this may limit the functionality of these systems. 3D printed gels have the advantage of being produced in shapes other than simply that of the vessel or mould in which they are prepared,[2] and they also enable the ability to form heterogenous constructs.[25] This contrasts with traditionally formed gels, which are usually homogenous in composition.[26] Tissue, a major goal for the bioprinting field,[27] is inherently heterogenous, so multi-layered systems wherein different layers comprise gels formed from different components are a significant step towards this goal.[28] This would enable variable mechanical properties throughout the construct,[29] which could be achieved by altering the gelator concentration in one type of gel or using multicomponent systems.[25]

Multi-layered systems built up from layers of printed supramolecular gels raise questions as to what happens at the boundaries between the extruded materials. Systems in which gelation occurs post extrusion may facilitate integration of gels formed near one another.[30] This would be expected to impact the mechanical properties across these border regions. Layers of varying mechanical properties formed from gels with differing gelator concentrations may not remain independent as the overall system, which is inherently dynamic in nature, homogenises through diffusion. This ambiguity is less likely within systems that are printed from preformed gels[20,25] where, due to the preservation of the pre-existing underlying gel network throughout the extrusion process, separately extruded materials would be expected to remain as such, even when 3D printed in close proximity.

We have previously reported a 3D printed multi-layered low molecular weight gel system in which heterogenous mechanical properties were imbued into different constituent gel layers

School of Chemistry, University of Glasgow, Glasgow, G12 8QQ, UK.
E-mail: dave.adams@glasgow.ac.uk

† Electronic supplementary information (ESI) available. See DOI: https://doi.org/10.1039/d2sm00663d

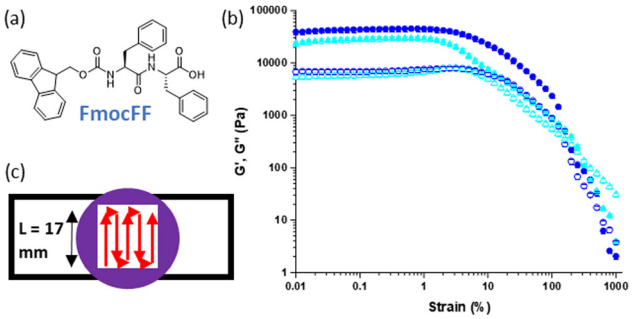

Fig. 1 (a) Chemical structure of FmocFF; (b) rheological strain sweeps comparing samples of single layers of unprinted (circles) and printed (triangles) of FmocFF gel (5 mg mL^{-1}, DMSO : H_2O 20%, printed at 4 μL mm^{-1}). G' is represented by filled shapes and G'' hollow shapes. Measurements were carried out on samples prepared in triplicate, with error bars representing the standard deviation derived from averaging the three subsequent results. (c) Cartoon diagram of gel extruded in a serpentine pattern to form a 3D printed layer.

by varying the concentration of the same gelator.[25] We used Fmoc-diphenylalanine (FmocFF), a well-known gelator and perhaps the most prominent example from the established Fmoc-dipeptide family of gelators (Fig. 1(a)).[31,32] It can be used to form hydrogels at physiological pH through a range of gelation triggers, such as solvent-switching and pH.[26,33–35] This enables potential applications in the biomedical field, such as cell culture or tissue engineering.[31,32,36] The 3D printing of solvent-triggered FmocFF hydrogels has previously been reported, with pre-formed FmocFF gels extruded from syringes *via* a modified 3D printer.[20] Moving beyond identical layers of gel, the system was extended to produce gel layers with different stiffness.[25] This enabled heterogenous mechanical properties within a sample, more closely mimicking natural tissue, which is inherently non-homogenous and can be achieved through different means.[27–29] Previously, the concentration of gelator, FmocFF, used to form gel layers was varied. A higher gelator concentration results in a stiffer gel due to the underlying fibrous network being more densely populated.[37] Both the number and relative positions of these stiffer gels layers were shown to be important to the overall mechanical properties of the sample.[25]

In this current work, we demonstrate 3D printed multi-layered systems containing gel layers formed from two different low molecular weight gelators (LMWGs) with differing mechanical properties. These give gels with distinct underlying microstructure and thus composition.

Results and discussion

We have previously demonstrated the successful 3D printing of LMWG based gels.[20,25] Here, an extrusion-based approach was used to print gels pre-formed within syringes into strips of gel which were then used to build up more complex shapes and patterns. Different triggers and parameters were explored and optimised, with solvent-triggered gels proving the most suitable for extrusion.

Initially, we printed preformed FmocFF gels and compared materials produced against unprinted equivalents with respect to their mechanical properties (Fig. 1(b)).[25] FmocFF gels could be shaped into layers of gel through printing in a serpentine pattern with a mould (Fig. 1(c)).[20]

This system was used to produce samples comprising multiple layers of printed FmocFF gels, where the addition of each successive layer was shown to increase the overall stiffness of the sample (see Fig. 4 below).[25]

Heterogenous mechanical properties and chemical composition within a layered sample were achieved through the incorporation of layers of gel formed from different gelators, each with an inherently different stiffness. In the absence of a definitive list of printable gelators, or even a guideline set of parameters that could suggest suitability for extrusion of these materials, we selected a known related gelator, 2NapFV, (Fig. 2) to be printed alongside FmocFF.[34] 2NapFV was found to be suitable for 3D printing after being formed *via* a DMSO : H_2O solvent-switch trigger within a syringe and extruded in an identical manner to FmocFF as outlined above.

Gels formed from 2NapFV are formed by self-assembly of the molecules into fibers which adopt a distinctly different microstructure from those produced from FmocFF, allowing them to be readily distinguished using confocal microscopy (Fig. 3).[34] This, alongside the fact that 2NapFV produces turbid gels whilst FmocFF gels are translucent, allows for easy visual identification of each material when analysing mixed samples across different length scales (Fig. 3).

The FmocFF gels triggered *via* a solvent-switch have a distinctly spherulitic-like network.[38] 2NapFV gels also present spherulitic networks but, under appropriate magnification, more uniform spanning fibers can be observed. These visual differences are accentuated after the extrusion process used to 3D print these materials. Here, the disappearance of spherulite-like domains within FmocFF gels can be seen (Fig. 3(b)-i and ii).

Using a 3-layered system, all combinations of the two different gels were examined as both printed and unprinted samples. These were formed within a mould and analysed *via*

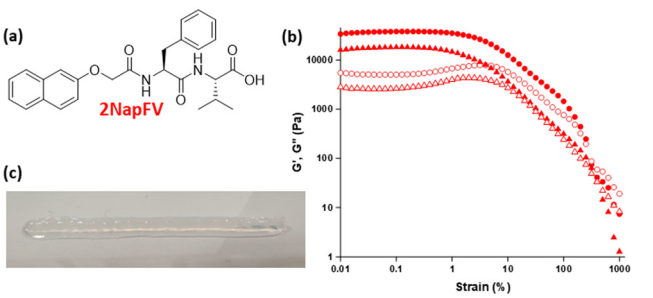

Fig. 2 (a) Chemical structure of 2NapFV. (b) Rheological strain sweeps comparing samples of single layers of unprinted (circles) and printed (triangles) 2NapFV gel (5 mg mL^{-1}, DMSO : H_2O 20%, printed at 4 μL mm^{-1}). G' is represented by filled shapes and G'' hollow shapes. Measurements were carried out on samples prepared in triplicate. Error bars representing the standard deviation derived from averaging the three subsequent results. (c) Image of a line of printed 2NapFV gel.

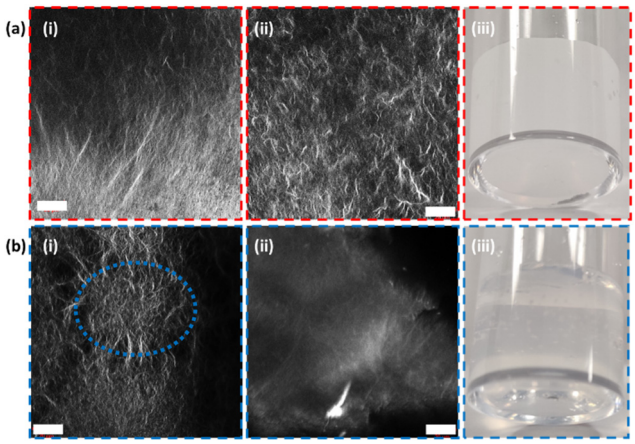

Fig. 3 Confocal microscopy of (a) 2NapFV & (b) FmocFF gels (5 mg mL^{-1}, DMSO : H_2O 20%, 400 μL, nile blue 2 μL mL^{-1} at 0.1 wt%) (i) unprinted and (ii) printed, alongside (iii) exemplar images of their differences in turbidity when formed as bulk gels. Scale bars (white) = 20 μm. An example of a spherulite-like domain is highlighted in blue for the unprinted FmocFF confocal image (bi).

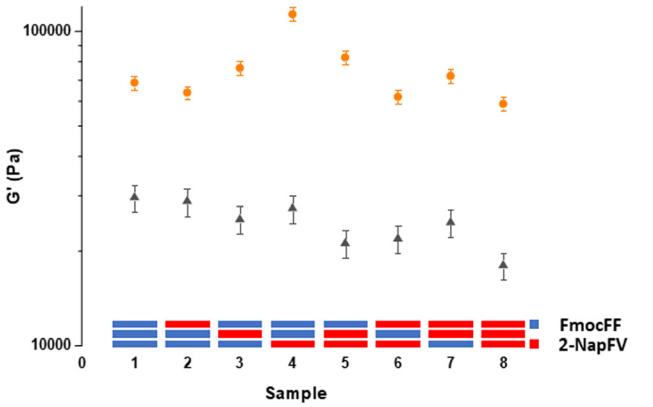

Fig. 5 Rheological G' values of multi-layered printed (triangles) and unprinted (circles) gel samples formed from FmocFF and 2NapFV gels (5 mg mL^{-1}, DMSO : H_2O 20%, printed at 4 μL mm^{-1}) with cartoon diagrams of sample layer composition shown. FmocFF gel layers are blue, whilst 2NapFV layers are red. Measurements were carried out on samples prepared in triplicate, with error bars representing the standard deviation derived from averaging the three subsequent results.

oscillatory rheology (Fig. 4 and 5).[20,25] Filaments of both 2NapFV and FmocFF gel were extruded in a serpentine pattern to achieve 3D printed layers of gel, which were built up to produce multi-layered printed samples (Fig. 4).

We highlight that since we are printing pre-gelled samples, each printed gel layer contains only a single gelator. Unprinted layers were cast directly in full height moulds as consecutive layers of solvent-switch triggered gels.[25] We also highlight that here we are focussing on three layers of printed gel whilst in Fig. 1 and 2 we used a single layer. As such, the absolute moduli differ for the pure gels in Fig. 1, 2 and 5.

Overall, the unprinted gel samples demonstrated consistently higher stiffness, with these values also being more reproducible than their printed counterparts. This is likely a result of the high stress exerted on the materials during the extrusion process. No clear trend is seen within unprinted samples comprising the two gels, with sample 4 being significantly stiffer than the rest of the set. The reason for this is unclear and may arise from how this specific combination of layers of gel integrate with one another and potentially the walls of the container. After printing, there is a general reduction in sample stiffness as we move from the majority of the gel layers being FmocFF to where a majority are 2NapFV layers. The printed set of multi-layered gels shows a greater difference in stiffness between samples comprising all FmocFF (Fig. 5, sample 1) and those which are all 2NapFV (Fig. 5, sample 8) than that seen in the unprinted set of samples. This increased discrepancy may indicate FmocFF to be more suitable for printing than 2NapFV.

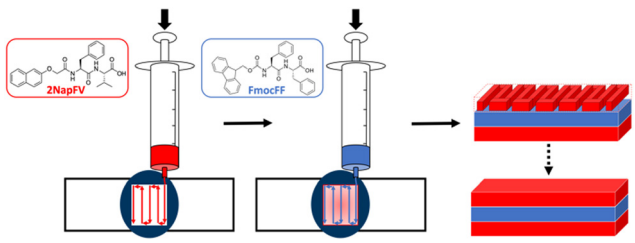

Fig. 4 Schematic diagram of formation of multi component 3D printed layered samples consisting of 2NapFV (red) and FmocFF (blue) gels.

To understand the printing process of layered systems in more detail, we examined the interface between the layers. Previously, some examples of 3D printed low molecular weight gels have been achieved through post-extrusion gelation, wherein baths of organic solvent or ionic solutions encourage gelation within extruded filaments upon leaving the printing nozzle, or shortly thereafter.[23,30] In these systems there is potential that material extruded in close proximity that is not yet fully gelled may amalgamate through the presence of interstrand crosslinks formed during gelation, similar to annealing demonstrated in some gels.[39] This could lead to a more uniform final material that displays augmented mechanical properties and may be able to better occupy the vessel in which it is printed but risks the loss of the programmed design and spatial control enabled through 3D printing.

Our system benefits from relying on the extrusion of preformed gels. FmocFF and related gels are thixotropic and demonstrate shear recovery, particularly when under a solvent-switch trigger and formed at high DMSO contents.[20] This is a result of the spherulite-like gelator network formed under these conditions allowing for the deformation and partial recovery of the pre-stressed structure upon removal of applied shear.[38,40] Due to the persistence of the underlying network created before extrusion in our system, gel filaments produced *via* this method would be expected to remain independent from neighbouring printed material, even when formed in very close proximity. Understanding what interactions are occurring, if any, at these points within samples is crucial. If distinct gel–gel boundaries are created in which a

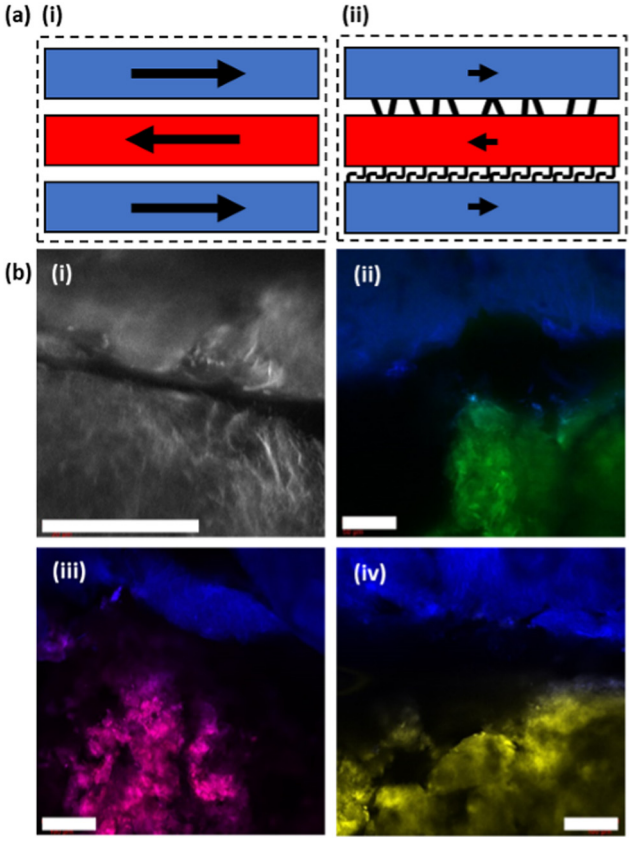

Fig. 6 (a) Schematic diagram of multi component 3D printed multi-layered samples in which layers have (i) preserved gel filament boundaries and (ii) interfacing between separately extruded material. (b) Multi-dyed confocal microscopy images of a boundary formed by printing 2NapFV (nile blue A, 2 μL mL^{-1} at 0.1 wt%, top) and FmocFF (nile blue A (i), fluorescein (ii), nile red (iii), thioflavin T (iv), 2 μL mL^{-1} at 0.1 wt%, bottom) gels (5 mg mL^{-1}, φ DMSO 0.2, 4 μL mm^{-1}) alongside each other. Scale bars (white) represent 100 μm.

clear border is preserved, then the gel layers within samples would be expected to act independently in response to applied stress (Fig. 6(a)-i). However, if the individual layers interface with neighbouring layers, then this could result in an additive effect on the overall mechanical properties, being greater than the sum of the contributions of the individual layers (Fig. 6(a)-ii).

Confocal microscopy was used to gain a better understanding of the interaction, or lack thereof, at the border between printed gel layers. Fluorescent dyes were incorporated into the gelation process to allow for the direct observation of printed gels and their underlying microstructure. These are usually hydrophobic molecules that are incorporated into the hydrophobic fibers formed during gelation. Initially the boundary between two printed strips of the same gel were imaged, but it proved difficult to accurately assign any observations.

Thus, filaments of 2NapFV gel printed in close proximity to FmocFF gels were imaged. Gels from these two gelators possess two clearly distinct microstructures by confocal microscopy, even after extrusion (as shown in Fig. 3). This should allow for a better picture to be painted as to the degree of interaction at printed borders (Fig. 6(b)). Using the same dye, nile blue A, for both 2NapFV and FmocFF gels printed in close proximity, the two unique microstructures can be clearly identified (Fig. 6(b)-i). 2NapFV maintains distinct fibers visible *via* confocal microscopy even after printing, whilst FmocFF becomes more homogenous and blurrier in appearance after printing (Fig. 6(b)-i, bottom and top, respectively). These are separated by a dark space, likely a solvent filled gap. Samples were thoroughly examined across different depths of field to further probe this partition. To the best of our knowledge, this gap remains free of printed material across samples, and can usually be followed the entire length of printed filaments, indicating that our printed gel filaments do remain independent and maintain a gel : gel boundary. This boundary remains clear of gel and would be expected to hinder transfer of material between gels.

To provide better contrast and increase certainty of a maintained printed border between gel layers, imaging was moved to a two-dye system (Fig. 6(b)-ii). Initially, fluorescein was incorporated into FmocFF gels whilst 2NapFV was labelled with nile blue A. This clearly distinguished the two separate gels and their respective microstructures, whilst confirming their position relative to one another. This system remained in agreement that an empty region was maintained between the two material borders. However, detail on the microstructure within the fluorescein-labelled FmocFF gels was lost as this is a hydrophilic dye. Therefore, it highlights the immobilised water content within the gel, whereas nile blue A is a hydrophobic dye, so is associated with the fibres of the gelator network. Whilst diffusion of fluorescein may be possible over an appropriate timescale, it remained localised to the gel in which it was initially incorporated within this experiment. To improve upon this, fluorescein was replaced by two lipophilic dyes, nile red and thioflavin T, within printed FmocFF gel for imaging (Fig. 6(b)-iii and (b)-iv respectively). These successfully reported on the microstructure of the FmocFF gels whilst continuing to suggest a lack of interaction between separately printed material formed from the different gelators. As such, these data show that the layers do not meld together but remain distinctly different. Whilst there seems to be some liquid between the layers, there is no sign of slipping in the rheology of the printed gels. There must be sufficient roughness on different length scales to ensure that slipping does not occur.

Conclusions

We have demonstrated the ability to 3D print multi-layered constructs in which the individual gel layers are formed from different gelators. This was achieved through the extrusion of preformed solvent-switch triggered gels rather than post-printing gelation. We have previously shown DMSO : H_2O triggered low molecular weight gels to be more suitable to 3D printing applications than pH triggered gels, owing to the different microstructure produced.[20] Both the overall composition and relative ordering of the different gel layers were shown

to be significant in determining the overall mechanical properties of multi-layered systems. The degree of interaction between printed gels was explored *via* confocal microscopy, with different underlying microstructures highlighted with different fluorescent dyes. Initial indications suggest that a distinct boundary between separately extruded material is maintained. This is expected to impact the overall mechanical properties of multi-layered printed gel systems. We hope this system shows the potential for further examples of multi-layered printed gels and provides insight towards future applications of these systems.

Experimental details

Preparation of LMWG solutions and gels

Low molecular weight gelators (LMWGs) FmocFF (F = phenylalanine) and 2NapFV (V = valine) were synthesized and used to form solvent-switch triggered hydrogels as previously outlined.[26,34] A known amount of gelator was dissolved in DMSO (at a concentration of 25 mg mL^{-1}), sonicated for 2 minutes, and diluted with water in one aliquot to give gels at a final gelator concentration of 5 mg mL^{-1}, and a volume fraction (φ) of DMSO of 0.2. Gels were either formed within, or extruded into, 3D printed plastic square shaped molds (19.5 × 19.5 × 5 mm, Fig. S1b, ESI†) adhered to a borosilicate glass microscope slide with Araldite®.[25] Gels were left overnight within a sealed hydrated environment before being printed or characterized.

Preparing unprinted multi-layered gels

For unprinted samples, layers of gel (1.065 mL) were formed directly within the mold. The gelator solution was pipetted in to give even coverage, with an aliquot of water gently pipetted in immediately after to trigger gelation. Each layer was left in a sealed vessel for 30 minutes before the addition of the next layer.[25]

3D printed gels

A modified RepRap Ormerod 2 (version 528.4) 3D printer was used to extrude 3D printed hydrogels.[20] Printed samples were formed by first making gels (2 mL) within polypropylene syringes. The syringes were then loaded into a custom gel 3D printer and used to print layers of pre-formed gel in a serpentine pattern at an extrusion rate of 4 μL mm^{-1} and a shear rate (γ) of 1500 s^{-1} (Fig. S1b and c, ESI†), as previously described.[20] Consecutive printed layers were added immediately after one another.

Rheological measurements

Samples for rheology were created by the sequential formation of either printed or non-printed layers of FmocFF and 2NapFV gels in different combinations.[20,25] Rheological measurements were carried out using a MCR 301 rheometer (Anton Paar), fitted with a cup and four-bladed vane geometry (ST10-4V-8.8/97.5-SN1910), and Rheoplus/32 v3.40 software. All measurements were carried out in triplicate, at 25 °C, with a measurement gap of 0.5 mm used.

G' values were taken as an average of those in the linear viscoelastic region from strain sweeps (strain = 0.01% to 1000%, frequency = 10 rad s^{-1}, T = 25 °C). The region within these plots at which G' and G'' remain constant under increasing strain up until the gel start to break and their values fluctuate significantly was defined as the linear viscoelastic region (LVER). The critical strain (γ_c) point at which the gel is said to have been broken is derived by the intersection between two tangents drawn from the LVER and post-LVER.

Confocal microscopy

For imaging, nile blue A, fluorescein, nile red and thioflavin T dyes (0.1 wt% aqueous solution, 2 μL per mL of gel) were incorporated into gels to allow for observation by confocal fluorescence microscopy using a Zeiss LSM 710 confocal microscope fitted with Zeiss N-Achroplan 10× and LD EC Epiplan NEUFLUAR 50× (0.55 DIC) objectives. Unprinted gels (5 mg mL^{-1}, 2 mL, φ DMSO 0.2) were formed directly within the well of Greiner Bio-one CELLview dishes. To study the microstructure of individual printed gels, single lines of either FmocFF or 2NapFV gel were printed directly onto standard microscope slides (Fig. S1a, ESI†). To probe the boundary between printed lines of gel, strips of FmocFF and 2-NapFV gel were printed on top of one another and then rotated 90°. For multi-dye imaging, 2-NapFV gels were formed with nile blue A dye incorporated and FmocFF gels with Fluorescein, nile red or thioflavin T.

Author contributions

Conceptualization, DJA; methodology, MH and DJA; formal analysis, MH; investigation, MH; resources, DJA; data curation, MH; writing-original draft preparation, MH and DJA; writing-review and editing, MH and DJA; supervision, DJA; project administration, DJA; funding acquisition, DJA. All authors have read and agreed to the published version of the manuscript.

Conflicts of interest

There are no conflicts to declare.

Acknowledgements

M. J. S. H. thanks the EPSRC for funding (EP/RS13222/1 and EP/T517896/1).

Notes and references

1 H. N. Chia and B. M. Wu, *J. Biol. Eng.*, 2015, **9**, 4.
2 T. Jungst, W. Smolan, K. Schacht, T. Scheibel and J. Groll, *Chem. Rev.*, 2016, **116**, 1496–1539.
3 N. A. Sather, H. Sai, I. R. Sasselli, K. Sato, W. Ji, C. V. Synatschke, R. T. Zambrotta, J. F. Edelbrock, R. R. Kohlmeyer, J. O. Hardin,

J. D. Berrigan, M. F. Durstock, P. Mirau and S. I. Stupp, *Small*, 2021, **17**, 2005743.
4 M. Rodrigues, A. C. Calpena, D. B. Amabilino, M. L. Garduño-Ramírez and L. Pérez-García, *J. Mater. Chem. B*, 2014, **2**, 5419.
5 S. Gupta, M. Singh, M. Amarendar Reddy, P. S. Yavvari, A. Srivastava and A. Bajaj, *RSC Adv.*, 2016, **6**, 19751–19757.
6 K. J. Skilling, F. Citossi, T. D. Bradshaw, M. Ashford, B. Kellam and M. Marlow, *Soft Matter*, 2014, **10**, 237–256.
7 X. Li, Y. Wang, C. Yang, S. Shi, L. Jin, Z. Luo, J. Yu, Z. Zhang, Z. Yang and H. Chen, *Nanoscale*, 2014, **6**, 14488–14494.
8 Y. Zhou and X. Li, *Chin. Chem. Lett.*, 2017, **28**, 1835–1840.
9 J. L. Drury and D. J. Mooney, *Biomaterials*, 2003, **24**, 4337–4351.
10 J. Li, R. Xing, S. Bai and X. Yan, *Soft Matter*, 2019, **15**, 1704–1715.
11 R. Suntornnond, J. An and C. K. Chua, *Macromol. Mater. Eng.*, 2017, **302**, 1600266.
12 L. Ouyang, C. B. Highley, C. B. Rodell, W. Sun and J. A. Burdick, *ACS Biomater. Sci. Eng.*, 2016, **2**, 1743–1751.
13 L. Ouyang, C. B. Highley, W. Sun and J. A. Burdick, *Adv. Mater.*, 2017, 29.
14 L. C. Hsiao, A. Z. Badruddoza, L. C. Cheng and P. S. Doyle, *Soft Matter*, 2017, **13**, 921–929.
15 L. Shi, H. Carstensen, K. Hölzl, M. Lunzer, H. Li, J. Hilborn, A. Ovsianikov and D. A. Ossipov, *Chem. Mater.*, 2017, **29**, 5816–5823.
16 Q. Liu, Q. Li, S. Xu, Q. Zheng and X. Cao, *Polymers*, 2018, **10**, 664.
17 C. B. Highley, C. B. Rodell and J. A. Burdick, *Adv. Mater.*, 2015, **27**, 5075–5079.
18 F. Andriamiseza, D. Bordignon, B. Payré, L. Vaysse and J. Fitremann, *J. Colloid Interface Sci.*, 2022, **617**, 156–170.
19 J. P. Schneider, D. J. Pochan, B. Ozbas, K. Rajagopal, L. Pakstis and J. Kretsinger, *J. Am. Chem. Soc.*, 2002, **124**, 15030–15037.
20 M. C. Nolan, A. M. Fuentes Caparros, B. Dietrich, M. Barrow, E. R. Cross, M. Bleuel, S. M. King and D. J. Adams, *Soft Matter*, 2017, **13**, 8426–8432.
21 H. H. Susapto, D. Alhattab, S. Abdelrahman, Z. Khan, S. Alshehri, K. Kahin, R. Ge, M. Moretti, A.-H. Emwas and C. A. E. Hauser, *Nano Lett.*, 2021, **21**, 2719–2729.
22 B. Raphael, T. Khalil, V. L. Workman, A. Smith, C. P. Brown, C. Streuli, A. Saiani and M. Domingos, *Mater. Lett.*, 2017, **190**, 103–106.
23 A. Chalard, M. Mauduit, S. Souleille, P. Joseph, L. Malaquin and J. Fitremann, *Addit. Manuf.*, 2020, **33**, 101162.
24 C. C. Piras, A. G. Kay, P. G. Genever, J. Fitremann and D. K. Smith, *Chem. Sci.*, 2022, **13**, 1972–1981.
25 A. M. Fuentes-Caparrós, Z. Canales-Galarza, M. Barrow, B. Dietrich, J. Läuger, M. Nemeth, E. R. Draper and D. J. Adams, *Biomacromolecules*, 2021, **22**, 1625–1638.
26 D. J. Adams, M. F. Butler, W. J. Frith, M. Kirkland, L. Mullen and P. Sanderson, *Soft Matter*, 2009, **5**, 1856.
27 M. P. Nikolova and M. S. Chavali, *Bioact. Mater.*, 2019, **4**, 271–292.
28 G. Liu, Z. Ding, Q. Yuan, H. Xie and Z. Gu, *Front. Chem.*, 2018, **6**, 439.
29 F. Yanagawa, S. Sugiura and T. Kanamori, *Regener. Ther.*, 2016, **3**, 45–57.
30 H. Jian, M. Wang, Q. Dong, J. Li, A. Wang, X. Li, P. Ren and S. Bai, *ACS Appl. Mater. Interfaces*, 2019, **11**, 46419–46426.
31 V. Jayawarna, M. Ali, T. A. Jowitt, A. F. Miller, A. Saiani, J. E. Gough and R. V. Ulijn, *Adv. Mater.*, 2006, **18**, 611–614.
32 A. Mahler, M. Reches, M. Rechter, S. Cohen and E. Gazit, *Adv. Mater.*, 2006, **18**, 1365–1370.
33 C. Tang, A. M. Smith, R. F. Collins, R. V. Ulijn and A. Saiani, *Langmuir*, 2009, **25**, 9447–9453.
34 L. Chen, S. Revel, K. Morris, L. C. Serpell and D. J. Adams, *Langmuir*, 2010, **26**, 13466–13471.
35 V. Jayawarna, S. M. Richardson, A. R. Hirst, N. W. Hodson, A. Saiani, J. E. Gough and R. V. Ulijn, *Acta Biomater.*, 2009, **5**, 934–943.
36 T. Liebmann, S. Rydholm, V. Akpe and H. Brismar, *BMC Biotechnol.*, 2007, **7**, 88.
37 F. M. Menger and K. L. Caran, *J. Am. Chem. Soc.*, 2000, **122**, 11679–11691.
38 X. Huang, S. R. Raghavan, P. Terech and R. G. Weiss, *J. Am. Chem. Soc.*, 2006, **128**, 15341–15352.
39 S. Panja, A. M. Fuentes-Caparros, E. R. Cross, L. Cavalcanti and D. J. Adams, *Chem. Mater.*, 2020, **32**, 5264–5271.
40 C. Yan, A. Altunbas, T. Yucel, R. P. Nagarkar, J. P. Schneider and D. J. Pochan, *Soft Matter*, 2010, **6**, 5143.